Front. Chem. Sci. Eng. 2020, 14(1): 28–40
https://doi.org/10.1007/s11705-019-1869-1

RESEARCH ARTICLE

Diporphyrin tweezer for multichannel spectroscopic analysis of enantiomeric excess

Daniel T. Payne (✉)[1], Mandeep K. Chahal[1], Václav Březina[2], Whitney A. Webre[3], Katsuhiko Ariga[1,4], Francis D'Souza[3], Jan Labuta (✉)[1], Jonathan P. Hill (✉)[1]

1 WPI Center for Materials Nanoarchitectonics, National Institute for Materials Science, Ibaraki 305-0044, Japan
2 Department of Macromolecular Physics, Faculty of Mathematics and Physics, Charles University, 18000 Prague, Czech Republic
3 Department of Chemistry, University of North Texas, Denton, TX 76203, USA
4 Department of Advanced Materials Science, Graduate School of Frontier Sciences, The University of Tokyo, Chiba 277-8561, Japan

Abstract Chiral 1,1'-binaphthyl-linked diporphyrin 'tweezers' (*R*)-**1**/(*S*)-**1** and the corresponding zinc(II) complexes (*R*)-**2**/(*S*)-**2** were prepared as chiral host molecules, and their utility for chiral analyses (especially enantiomeric excess (*ee*) determinations) were evaluated. Tris(1-*n*-dodecyl)porphyrins were used for the first time as the interacting units. Host capabilities of the diporphyrin tweezers were investigated by titrations with (*R*,*R*)- and (*S*,*S*)-cyclohexane-1,2-diamine (CHDA). The host molecules could be used as multichannel probes of *ee* by using UV-vis, circular dichroism (CD), fluorescence emission and ^{1}H nuclear magnetic resonance (^{1}H-NMR) methods. Chiral configurations could also be differentiated using CD or ^{1}H-NMR spectroscopy. All three optical techniques give good resolution of *ee* with reasonable sensitivity considering the low concentrations used (ca. 10^{-6} mol·L^{-1}). The *ee* determination of CHDA enantiomers using NMR spectroscopy is also possible because of the reasonably well separated resonances in the case of (*R*,*R*)- and (*S*,*S*)-CHDA. Non-metallated (*R*)-**1**/(*S*)-**1** hosts could not be used to detect chiral information in a strongly acidic chiral guest. This work demonstrates the utility of 1,1'-binaphthyl-linked chiral hosts for chiral analysis of ditopically interacting enantiomers.

Keywords porphyrin dimer, chirality, enantiomeric excess, CD, fluorescence

1 Introduction

Chirality is a key aspect of the modern chemical sciences and its analysis is critical in several disciplines including pharmaceutical sciences [1], molecular recognition [2] and asymmetric catalysis [3]. Enantiomeric excess (*ee*) is an invaluable parameter for the estimation of the success of chemical processes occurring in these fields since it defines the purity of non-racemic mixtures of chiral compounds. It is usually defined as:

$$ee = \frac{[R]_t - [S]_t}{[R]_t + [S]_t}, \quad (1)$$

where $[R]_t$ and $[S]_t$ are the respective total analytical concentrations of the (*R*)- and (*S*)-enantiomers of analyte (guest). Several methods have been introduced for its analysis including high performance liquid chromatography [4] and nuclear magnetic resonance (NMR) spectroscopy [5] whose protocols can also include chiral derivatization to improve differentiation of enantiomers. These methods are well established and widely used but can be time consuming and costly if the required reagents or equipment are not immediately available. Therefore, the development of new methodologies for the determination of *ee* is of significant current interest [6]. Calibrated optical methods involving circular dichroism (CD) can be extremely powerful methods for analysis of chiral parameters such as *ee* [7]. There are also many other reported methods based on interactions of chiral probe molecules with chiral analytes, which usually rely on diastereomer formation — so-called chiral solvating agents [8]. A successful example of this is α-trifluoromethyl-9-anthracenemethanol [9] although there are many commercially available compounds that can be operated as chiral solvating agents. They are especially useful for the

Received November 8, 2018; accepted May 20, 2019

E-mails: daniel.tony.payne@gmail.com (Payne D T), Labuta.Jan@nims.go.jp (Labuta J), Jonathan.Hill@nims.go.jp (Hill J P)

assessment of *ee* using NMR spectroscopy, and methods even exist using achiral molecules as the probe species [10,11]. The latter is important for the monitoring of asymmetric reactions since the achiral probe would not influence the outcome of the reaction from the point-of-view of its chirality.

On the other hand, porphyrins [12] are a well-studied family of compounds containing a tetrapyrrole macrocycle, whose wide synthetic flexibility has led to their study for asymmetric catalysis [13] or as chiral receptors [14]. Most of that work has been accomplished using porphyrin monomer species containing a single macrocyclic unit. A particular class of porphyrin molecules for analysis of chirality exists in the 'bisporphyrin tweezer' molecules whose form and function have been studied since the initial reports of a CD signature in a porphyrin-binaphthyl conjugate molecule by Ema et al. [15] and Hayashi et al. in the mid-1990s [16]. Subsequently, it has been found that both achiral and chiral bisporphyrin tweezers can act as chiral recognition molecules. Typical examples of achiral tweezers include the diester-linked tetraphenylporphyrin dimer introduced by Berova, Nakanishi and coworkers [17] and the *β*-octaethylporphyrin dimer extensively studied by Borovkov, Inoue and coworkers [18]. In addition, several examples of bisporphyrin tweezers containing chiral linkages are known [19] where the chirality of linkage affects the conformation of the guest binding site introducing some selectivity of guest chirality [20]. These molecules might be useful not only for guest enantiomer determination and *ee* estimation but also for applications in chiral separations based on stereoisomer differentiation.

Our recent work in this area is based on observations that some weakly interacting achiral host molecules such as N_{21},N_{22}-dibenzyl-5,10,15,20-tetrakis(3,5-di-*t*-butyl-4-oxocyclohexadien-2,5-ylidenyl)porphyrinogen (Bn_2OxP) [10], *meso*-tetraphenylporphyrin dications [21] or even simple benzylamine [22] can be used effectively as probes of *ee* for a wide variety of guests including amino acid derivatives, *α*-hydroxy carboxylic acids and some proprietary pharmaceuticals. They operate as prochiral probes leading to them being referred to as prochiral chiral solvating agents (pro-CSA). Our previous work has prompted us to consider molecular design as a means for extending or improving the properties of the compounds used as chiral probes. Therefore, in this study we have designed a probe molecule (Fig. 1) with the following chemical features: (1) an intrinsically chiral moiety (to make possible stereoisomer differentiation), (2) porphyrin units for guest interactions (by protonation or transition metal coordination), (3) *meso*-alkylporphyrins proposed to improve host-guest binding strength (reduced steric hindrance between binding units) and (4) bisporphyrin tweezers. The key novelty here is the use of *meso*-*n*-alkyl porphyrins whose properties vary from the often used tetraphenylporphyrins. *Meso*-*n*-alkylporphyrins [23] are usually not considered because of perceived difficulties in their (low yield) syntheses although there now exist effective methods for their preparation in moderate yield [24].

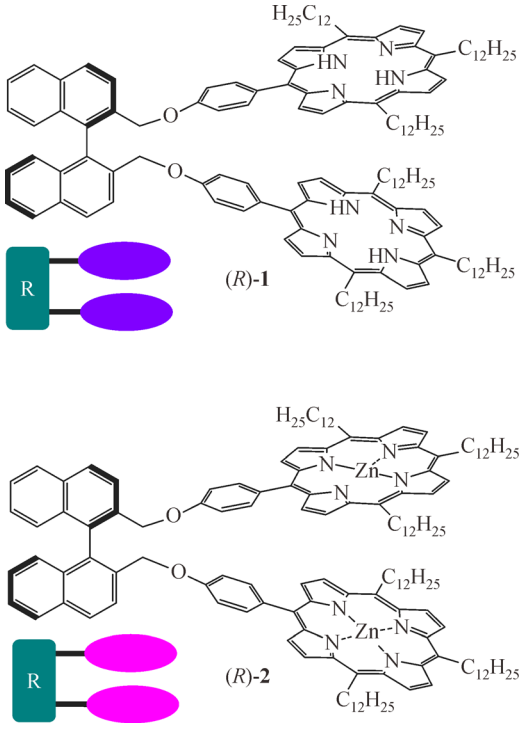

Fig. 1 Sensors developed in this study. Chemical structures and schematic representations of 1,1'-binaphthyl-based bisporphyrin tweezers used in this work. Top: metal free ((*R*)-**1**) and (bottom) its zinc complex ((*R*)-**2**).

2 Experimental

2.1 General

Reagents and dehydrated solvents (in septum-sealed bottles) used for syntheses and spectroscopic measurements were obtained from Tokyo Kasei Chemical Co., Wako Chemical Co. or Aldrich Chemical Co. and were used without further purification. Electronic absorption spectra were measured using a JASCO V-570 ultraviolet–visible (UV-Vis)/near-infrared spectrophotometer. Fluorescence spectra were measured using a JASCO FP-670 spectrofluorimeter. Fourier-transform infrared spectroscopy (FTIR) spectra were obtained from solid samples using a Thermo-Nicolet 760X FTIR spectrophotometer equipped with ATR accessory. CD spectra were measured using a JASCO J-820 Spectropolarimeter. UV-Vis, CD and fluorescence emission spectra were recorded at 1 nm data point intervals at 200 $nm \cdot min^{-1}$ scan rate at the instrumentations standard sensitivity settings. ^{1}H NMR spectra were recorded on a JEOL AL300BX NMR spectrometer at 300 MHz, proton decoupled ^{13}C NMR

spectra were recorded at 76 MHz on a JEOL AL300BX NMR spectrometer at the stated temperatures. Data was processed on Delta version 5.0.5.1 and Always JNM-AL version 6.2. ^{1}H NMR chemical shifts (δ) are reported in ppm relative to tetramethylsilane for $CDCl_3$ ($\delta = 0.00$ ppm) or the residual solvent peak for other solvents. ^{13}C NMR chemical shifts (δ) are reported in ppm relative to the solvent reported. Coupling constants (J) are expressed in Hertz (Hz), shift multiplicities are reported as singlet (s), doublet (d), triplet (t), quartet (q), double doublet (dd), multiplet (m) and broad singlet (bs). Matrix–assisted laser desorption/ionization time–of–flight mass spectra (MALDI–TOF–MS) were measured using a Shimadzu-Kratos model Axima CFR + mass spectrometer with dithranol as matrix.

General procedure for spectroscopy measurements: Guest solutions (3.5×10^{-4} mol·L^{-1}) in the relevant solvent were added to a solution of host (3.5 mL, 1.0×10^{-6} mol·L^{-1}) in the relevant solvent in a 1 cm path length quartz cell with 4 polished faces at room temperature and recorded immediately.

2.2 Synthesis of chiral diporphyrin tweezers

5-(4-Methoxyphenyl)-10,15,20-tris(1-n-dodecyl)porphyrin (**3**). Montmorillonite K10 (21.0 g) was activated by heating at 140°C under reduced pressure for 2 h in a 3 L reaction vessel. It was then allowed to cool to room temperature and suspended in anhydrous dichloromethane (2.0 L). Tridecanal (7.1 mL, 30.0 mmol, 0.5 equiv.) and 4-anisaldehyde (3.7 mL, 30.0 mmol, 0.5 equiv.) dissolved in anhydrous dichloromethane (20 mL) were added and the mixture was degassed by purging with dry nitrogen. Pyrrole (4.1 mL, 60 mmol, 1 equiv.) was added and the reaction was stirred for 40 h at room temperature under a nitrogen atmosphere with light excluded. 2,3-Dichloro-5,6-dicyano-*p*-benzoquinone (10.5 g, 46 mmol, 0.75 equiv.) was added and the reaction was heated to reflux for 2 h. The reaction mixture was filtered through Celite and the filtrate solvent was removed under reduced pressure. The crude residue was purified by column chromatography (Al_2O_3; CH_2Cl_2/*n*-hexane 35:65, then SiO_2, CH_2Cl_2/*n*-hexane 35:65) to give the desired compound **3** (1.1 g, 7.6%). ^{1}H NMR (300 MHz, $CDCl_3$, δ): 9.51 (dd, $J = 8.6$, 4.9 Hz, 4H), 9.37 (d, $J = 4.8$ Hz, 2H), 8.83 (d, $J = 5.1$ Hz, 2H), 8.07 (d, $J = 8.4$ Hz, 2H), 7.26–7.31 (m, 2H), 4.91–5.01 (m, 6H), 4.11 (s, 3H), 2.44–2.60 (m, 6H), 1.74–1.85 (m, 6H), 1.25–1.47 (m, 48H), 0.84–0.89 (m, 9H), –2.66 (s, 2H) ppm. ^{13}C NMR (76 MHz, $CDCl_3$, δ): 159.2, 135.4, 135.0, 119.2, 119.0, 117.8, 112.0, 55.6, 38.9, 38.7, 35.5, 31.9, 30.7, 30.6, 29.7, 29.7, 29.6, 29.3, 22.7, 14.1 ppm. IR (ATR): 1607 (C = C str.), 2850–2920 (C–H str.), 3318 (N–H str.) cm^{-1}. MALDI-TOF-MS (dithranol): calcd for $C_{63}H_{93}N_4O$ $[M + H]^+$ 921.75; found 921.51.

5-(4-Hydroxyphenyl)-10,15,20-tris(1-n-dodecyl)porphyrin (**4**). Boron tribromide in dichloromethane (17% w/v, 3.5 mL) was added with stirring to a solution of **3** (0.70 g, 0.76 mmol, 1 equiv.) in dichloromethane (70 mL) at 0°C. The reaction was allowed to warm to room temperature then stirred for 2 h. The reaction mixture was quenched with methanol (30 mL), washed with water then saturated aqueous 1 mol·L^{-1} potassium carbonate solution, dried over sodium sulfate and filtered. The solvents were removed under reduced pressure and the crude residue was purified by column chromatography (SiO_2, 0.5% methanol in DCM) to afford the desired compound **4** (0.68 g, 98%). ^{1}H NMR (300 MHz, $CDCl_3$, δ): 9.46 (dd, $J = 8.6$, 5.0 Hz, 4H), 9.33 (d, $J = 4.8$ Hz, 2H), 8.78 (d, $J = 4.8$ Hz, 2H), 7.94 (d, $J = 8.1$ Hz, 2H), 7.03 (d, $J = 8.3$ Hz, 2H), 4.86–4.96 (m, 6H), 2.43–2.53 (m, 6H), 1.71–1.82 (m, 6H), 1.25–1.48 (m, 48H), 0.84–0.87 (m, 9H), –2.66 (bs, 2H) ppm. ^{13}C NMR (76 MHz, $CDCl_3$, δ): 155.2, 135.4, 135.1, 131.0, 128.4, 119.2, 119.1, 117.7, 113.5, 38.9, 38.7, 35.8, 35.4, 31.9, 30.7, 30.6, 29.7, 29.6, 29.4, 22.7, 14.1 ppm. IR (ATR): 1608 (C = C str.), 2850–2920 (C–H str.), 3316 (N–H str.), 3325 (O–H str.) cm^{-1}. MALDI-TOF-MS (dithranol): calcd for $C_{62}H_{92}N_4O$ $[M + 2H]^+$ 908.73; found 908.35.

(R)-2,2′-Bis((4-(10,15,20-tridodecylporphyrin-5-yl)phenoxy)methyl)-1,1′-binaphthalene ((*R*)-**1**). (*R*)-2,2′-Bis(bromomethyl)-1,1′-binaphthyl (40 mg, 0.091 mmol, 1 equiv.), **4** (200 mg, 0.22 mmol, 2.4 equiv.) and potassium carbonate (100 mg, 0.72 mmol, 8 equiv.) were dissolved in anhydrous acetone (5 mL) and refluxed for 18 h under a nitrogen atmosphere. The reaction was cooled to room temperature and the solvent removed under reduced pressure. The crude residue was purified by column chromatography (SiO_2, 60%–80% DCM in hexane) to afford the desired compound (*R*)-**1** (146 mg, 63%). ^{1}H NMR (300 MHz, $CDCl_3$, δ): 9.38 (d, $J = 5.0$ Hz, 4H), 9.09 (d, $J = 4.4$ Hz, 4H), 8.68 (d, $J = 4.8$ Hz, 4H), 8.58 (d, $J = 4.8$ Hz, 4H), 8.29 (d, $J = 8.6$ Hz, 2H), 8.22 (d, $J = 8.4$ Hz, 2H), 8.13 (d, $J = 8.3$ Hz, 2H), 7.95 (d, $J = 8.6$ Hz, 4H), 7.59–7.64 (m, 2H), 7.39–7.48 (m, 4H), 7.23 (d, $J = 8.4$ Hz, 4H), 5.40 (d, $J = 12.7$ Hz, 2H), 5.26 (d, $J = 12.5$ Hz, 2H), 4.92–4.97 (m, 4H), 4.09 (d, $J = 6.6$ Hz, 6H), 2.56–2.66 (m, 4H), 1.84–2.05 (m, 12H), 1.58–1.65 (m, 4H), 1.21–1.47 (m, 100H), 0.90–0.94 (m, 18H), –3.01 (s, 4H) ppm. ^{13}C NMR (76 MHz, $CDCl_3$, δ): 158.2, 135.7, 135.2, 134.0, 133.6, 133.4, 132.9, 129.0, 128.4, 126.9, 126.4, 126.1, 126.0, 118.8, 118.5, 117.5, 113.0, 68.5, 39.0, 38.3, 35.8, 34.8, 32.0, 31.9, 31.6, 30.8, 30.3, 29.9, 29.8, 29.8, 29.7, 29.7, 29.7, 29.6, 29.5, 29.4, 29.4, 22.7, 22.7, 14.2 ppm. IR (ATR): 1605 (C = C), 2850–2920 (CH), 3315 (NH) cm^{-1}. MALDI-TOF-MS (dithranol): calcd for $C_{146}H_{194}N_8O_2$ $[M]^+$ 2091.53; found 2091.43 $[M]^+$.

(S)-2,2′-Bis((4-(10,15,20-tridodecylporphyrin-5-yl)phenoxy)methyl)-1,1′-binaphthalene ((*S*)-**1**). This compound was prepared using the same method as for (*R*)-**1**. Yield: 65 mg, 57%. ^{1}H NMR (300 MHz, $CDCl_3$, δ): 9.38 (d, $J = 4.6$ Hz, 4H), 9.09 (d, $J = 3.9$ Hz, 4H), 8.67 (d, $J = 4.8$ Hz, 4H), 8.55 (d, $J = 4.8$ Hz, 4H), 8.28 (d, $J = 8.6$ Hz, 2H), 8.21 (d, J

= 8.6 Hz, 2H), 8.12 (d, *J* = 8.3 Hz, 2H), 7.93 (d, *J* = 8.4 Hz, 4H), 7.61 (t, *J* = 7.0 Hz, 2H), 7.36–7.46 (m, 4H), 7.22 (d, *J* = 8.4 Hz, 4H), 5.37 (d, *J* = 12.7 Hz, 2H), 5.24 (d, *J* = 12.5 Hz, 2H), 4.95 (t, *J* = 7.7 Hz, 4H), 4.09 (d, *J* = 7.2 Hz, 6H), 2.59 (d, *J* = 6.1 Hz, 4H), 1.83–2.04 (m, 12H), 1.58–1.68 (m, 4H), 1.19–1.30 (m, 100H), 0.86–0.96 (m, 18H), –3.03 (s, 4H) ppm. ^{13}C NMR (76 MHz, $CDCl_3$, *δ*): 158.3, 135.6, 135.2, 134.1, 133.7, 133.5, 132.9, 129.0, 128.4, 126.9, 126.4, 126.1, 126.0, 118.8, 118.6, 117.5, 113.0, 68.5, 39.0, 38.3, 35.8, 34.8, 31.9, 30.8, 30.3, 29.8, 29.8, 29.8, 29.6, 29.6, 29.5, 29.4, 29.4, 22.7, 14.1 ppm. IR (ATR): 1605 (C = C str.), 2850–2920 (C–H str.), 3316 (N–H str.) cm^{-1}. MALDI-TOF-MS (dithranol): calcd for $C_{146}H_{194}N_8O_2$ $[M]^+$ 2091.53; found 2091.57.

(R)-2,2'-Bis((4-(10,15,20-tridodecylporphinatozinc-5-yl)phenoxy)methyl)-1,1'-binaphthalene ((*R*)-**2**). Zinc (II) acetate dihydrate (50 mg, 0.27 mmol) dissolved in methanol (5 mL) was added dropwise to a solution of (*R*)-**2** (100 mg, 4.78 × 10^{-5} mol) in chloroform (15 mL) and the resulting mixture was shielded from light and refluxed for 3 h under an atmosphere of dry nitrogen. The reaction mixture was allowed to cool and solvents removed under reduced pressure. The resulting residue was dissolved in dichloromethane and passed through a short column of Al_2O_3 eluting with dichloromethane. A minor low polarity byproduct eluting first was discarded. (*R*)-**2** containing fractions were combined and dried over anhydrous Na_2SO_4. The solution was then filtered and solvents removed under reduced pressure giving (*R*)-**2** as a dark purple sticky solid with slight green secondary coloration. Yield: 100 mg, 95%. ^{1}H NMR (300 MHz, $CDCl_3$, *δ*): 8.85 (d, *J* = 4.4 Hz, 4H), 8.35 (d, *J* = 4.0 Hz, 4H), 8.26 (d, *J* = 8.4 Hz, 2H), 8.18 (d, *J* = 8.8 Hz, 2H), 8.07–8.12 (m, 8H), 7.61 (t, *J* = 8.6 Hz, 6H), 7.42 (t, *J* = 7.7 Hz, 2H), 7.30 (d, *J* = 8.4 Hz, 4H), 7.19 (d, *J* = 8.4 Hz, 4H), 5.34 (d, *J* = 13.6 Hz, 2H), 5.26 (d, *J* = 14.3 Hz, 2H), 4.54–4.72 (m, 4H), 3.20–3.34 (m, 8H), 2.38–2.49 (m, 4H), 1.82–1.94 (m, 12H), 1.30–1.53 (m, 104H), 0.87–0.92 (m, 18H) ppm. ^{13}C NMR (76 MHz, $CDCl_3$, *δ*): 157.5, 148.4, 148.1, 147.7, 147.7, 136.9, 135.1, 133.9, 133.4, 133.0, 133.0, 131.0, 129.1, 128.5, 127.7, 127.3, 127.0, 126.5, 126.3, 125.7, 125.6, 119.2, 118.3, 118.2, 112.7, 67.7, 39.1, 38.5, 35.7, 34.2, 32.0, 31.0, 30.7, 29.9, 29.9, 29.8, 29.8, 29.7, 29.7, 29.6, 29.4, 22.7, 14.1 ppm. IR (ATR): 1605 (C = C str.), 2850–2920 (C–H str.) cm^{-1}. MALDI-TOF-MS (dithranol): calcd for $C_{146}H_{192}N_8O_2Zn_2$ $[M + 2H]^+$ 2217.38; found 2217.22.

(S)-2,2'-Bis((4-(10,15,20-tridodecylporphinatozinc-5-yl)phenoxy)methyl)-1,1'-binaphthalene ((*S*)-**2**). This compound was prepared using the same method as for (*R*)-**2**. Yield: 55 mg, 95%. ^{1}H NMR (300 MHz, $CDCl_3$, *δ*): 8.85 (d, *J* = 4.8 Hz, 4H), 8.35 (d, *J* = 4.0 Hz, 4H), 8.26 (d, *J* = 8.8 Hz, 2H), 8.18 (d, *J* = 8.8 Hz, 2H), 8.07–8.12 (m, 8H), 7.58–7.64 (m, 6H), 7.39–7.45 (m, 2H), 7.30 (d, *J* = 8.4 Hz, 4H), 7.19 (d, *J* = 8.8 Hz, 4H), 5.34 (d, *J* = 13.2 Hz, 2H), 5.26 (d, *J* = 13.9 Hz, 2H), 4.49–4.72 (m, 4H), 3.20–3.37 (m, 8H), 2.37–2.45 (m, 4H), 1.82–1.93 (m, 12H), 1.30–1.53 (m, 105H), 0.87–0.92 (m, 18H) ppm. ^{13}C NMR (76 MHz, $CDCl_3$, *δ*): 157.5, 148.4, 148.1, 147.7, 147.7, 136.9, 135.1, 133.9, 133.4, 133.0, 133.0, 131.0, 129.1, 128.5, 127.7, 127.3, 127.0, 126.5, 126.3, 125.7, 125.6, 119.2, 118.3, 118.2, 112.7, 67.7, 39.1, 38.5, 35.8, 34.2, 32.0, 31.0, 30.7, 29.9, 29.9, 29.8, 29.8, 29.7, 29.6, 29.6, 29.4, 22.7, 14.1 ppm. IR (ATR): 1604 (C = C str.), 2850–2920 (C–H str.) cm^{-1}. MALDI-TOF-MS (dithranol): calcd for $C_{146}H_{192}N_8O_2Zn_2$ $[M + H]^+$ 2217.38; found 2216.60.

3 Results and discussion

The synthetic route of (*R*)-**1** and (*R*)-**2** is outlined in Scheme 1. Porphyrin precursors were synthesized by the acid catalyzed condensation of pyrrole with tridecanal/4-methoxybenzaldehyde using activated K10 Montmorillonite clay as catalyst in dichloromethane followed by oxidation with 2,3-dichloro-5,6-dicyano-1,4-benzoquinone (DDQ). Porphyrinic products were separated by column chromatography. Following its isolation, 5-(4-methoxyphenyl)-10,15,20-tris(*n*-dodecyl)porphyrin (**3**) was demethylated using boron tribromide. Host molecules (*R*)-**1** and (*S*)-**1** were prepared by reaction of the resulting 4-hydroxyphenyl-substituted *meso*-trialkylporphyrin (TAP, **4**) with the respective 2,2'-di(bromomethyl)-1,1'-binaphthyl precursor. Zinc complexation to give (*R*)-**2** and (*S*)-**2** was performed similarly to a literature method [25]. Sensors (*R*)-**1**/(*S*)-**1** and (*R*)-**2**/(*S*)-**2** were both also purified by gel permeation chromatography over Biobeads SX-1.

Since we have previously found some *ee* sensing activity in porphyrin dications [21], we initially investigated the interactions between (*R*)-**1** and camphorsulfonic acid (CSA) according to the schemes shown in Fig. 2. However, we found no chiral selectivity of binding between the two enantiomers of CSA suggesting that there is no complexation between protonated host and CSA counteranions most likely for reasons of inter-dication electrostatic repulsion and the lack of any specific clustering with the counteranions. The UV-vis spectroscopic data in Fig. 2 show highly cooperative tetraprotonation of (*R*)-**1** host. A 1:4 host-guest binding model [10,26,27] (cf. Electronic Supplementary Material, ESM) was proven using a Job's plot (Fig. 2(c)) with maximum at x_H = 0.2. Using this model we estimated the overall binding constants (Table S1) as determined by UV-vis (Figs. 2(a) and 2(b)) and fluorescence emission spectroscopic data (Fig. S1, cf. ESM)). The analysis of 1:4 binding isotherm together with singular value decomposition (SVD) procedure [28–33] applied on the UV-vis spectra of the titration experiments (Figs. S8 and S9 (cf. ESM)) show that only two species (Fig. 2(d)) are present during the whole titration. This is represented by a significant decrease of 'numeric value' (a measure of significance in SVD analysis) in Fig. 2(d) for singular values higher then

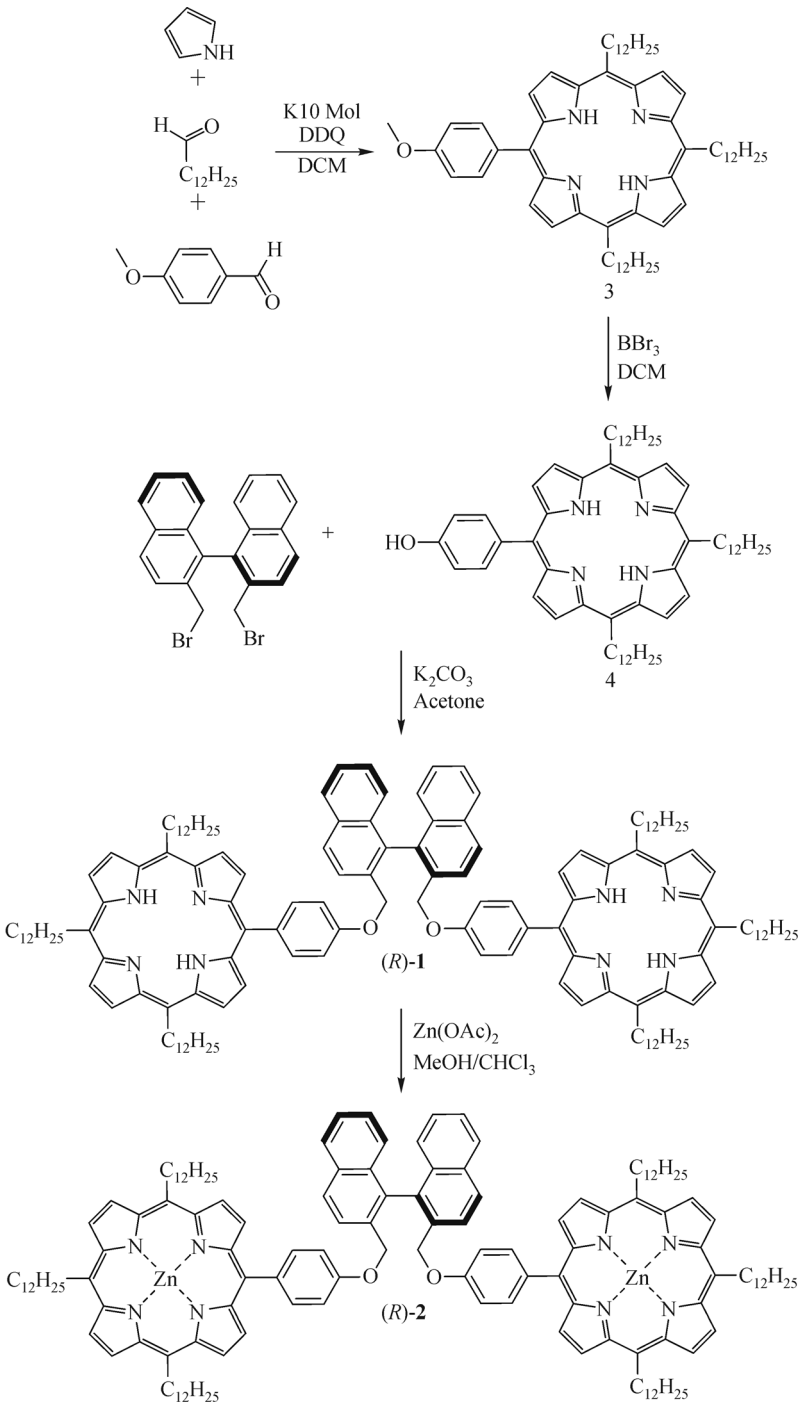

Scheme 1 Synthesis of diporphyrin tweezers (*R*)-**1** and (*R*)-**2**.

two (cf. ESI). This also means that only free (*R*)-**1** host (H) and ((*R*)-CSA)$_4$⊂(*R*)-**1** tetraprotonated complex (HG$_4$) can be spectroscopically observed. Other species, such as ((*R*)-CSA)$_3$⊂(*R*)-**1** (HG$_3$), ((*R*)-CSA)$_2$⊂(*R*)-**1** (HG$_2$) and (*R*)-CSA⊂(*R*)-**1** (HG), are not detectable, which also suggests a high positive binding cooperativity. Based on these analyses, only overall binding constants $\beta_4 = K_1K_2K_3K_4$ for complexation of CSA with (*R*)-**1** (see Table S1) could be estimated. The protonation of (*R*)-**1** by CSA does not induce any observable CSA enantiomer dependent response in the CD spectrum of (*R*)-**1** (Fig. S2, cf. ESM). Temperature is often the controlling factor in interactions involving analytes and porphyrin dications [21] making it necessary to optimize measurement technique and parameters to detect chirality specific phenomena.

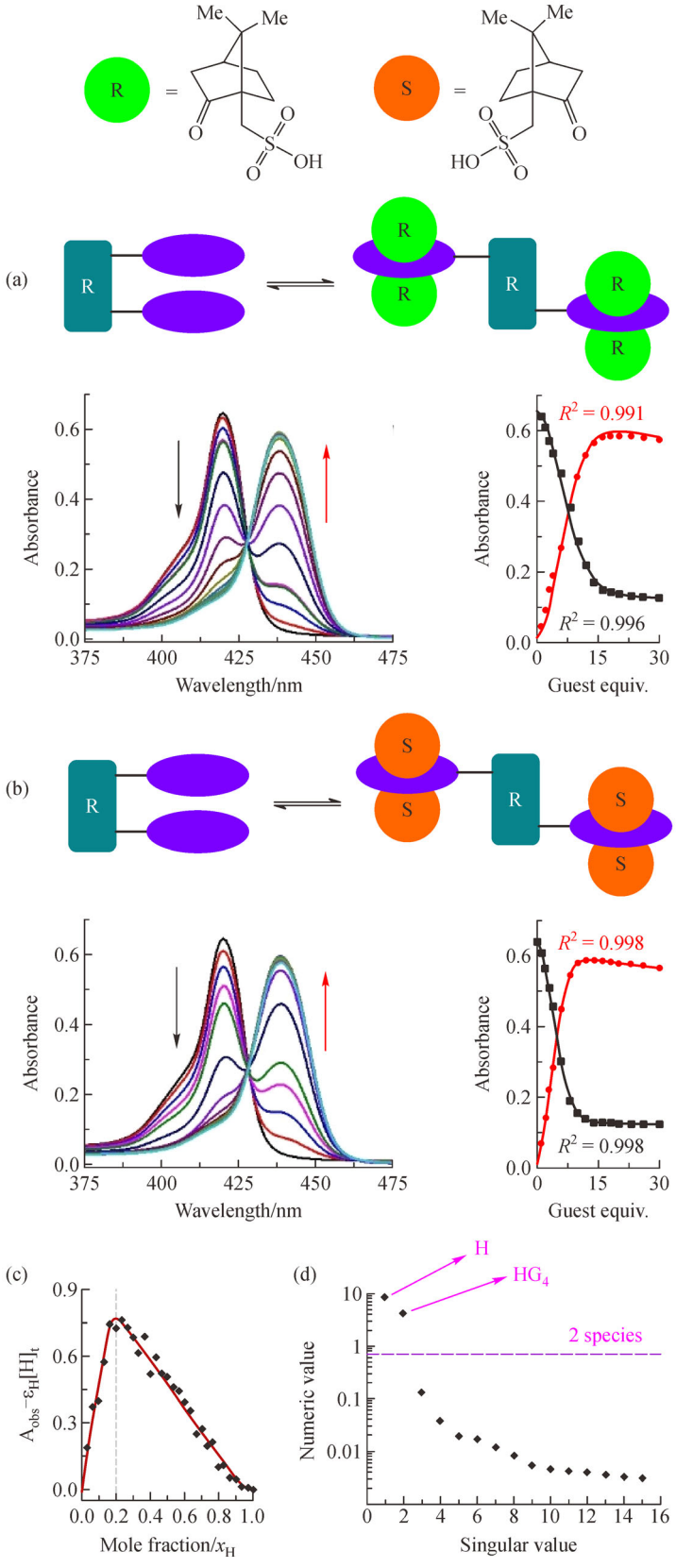

Fig. 2 Titrations of (*R*)-**1** monitored by UV-vis spectroscopy. (a) Titration of (*R*)-**1** (1.0×10^{-6} mol·L^{-1}) with 0–30 equiv. of (*R*)-CSA (3.5×10^{-4} mol·L^{-1}) in chloroform monitored by UV-vis spectroscopy at room temperature and 1:4 host-guest binding isotherms for the titration of (*R*)-**1** with (*R*)-CSA. The binding isotherms were constructed from absorbances at 420 nm (black) and 440 nm (red) and fitted simultaneously. (b) Titration of (*R*)-**1** (1.0×10^{-6} mol·L^{-1}) with 0–30 equiv. of (*S*)-CSA (3.5×10^{-4} mol·L^{-1}) in chloroform monitored by UV-vis spectroscopy at room temperature and 1:4 host-guest binding isotherms for the titration of (*R*)-**1** with (*S*)-CSA. The binding isotherms were constructed from absorbances at 420 nm (black) and 440 nm (red) and fitted simultaneously. For actual binding constants see Table S1. (c) Job's plot constructed for the binding of (*R*)-CSA with (*R*)-**1** (the total concentration was kept constant at $[H]_{tot} + [G]_{tot} = 10^{-5}$ mol·L^{-1}) in chloroform monitored at 440 nm at room temperature. *x*-axis shows molar fraction of host $x_H = [H]_{tot} / ([H]_{tot} + [G]_{tot})$. The red curve is 1:4 calculated Job's plot using $\beta_4 = 1.22 \times 10^{21}$ M^{-4} (Table S1). (d) Singular values as obtained from singular value decomposition of titration (*R*)-CSA into (*R*)-**1** solution.

In order to test the potential for tighter binding of chiral analyte species, we complexed the porphyrin macrocycles of (*R*)-**1**/(*S*)-**1** with zinc(II) cations. This enables us to assess the binding of chiral ditopic guests with stereoisomers of 1,2-cyclohexanediamine (CHDA) being selected as typical model guests because of its known propensity to interact with similar bisporphyrin tweezers [34,35] (other molecular probes for CHDA *ee* analysis are also known [36–39]) and because of uniformity of binding constants over the two host sites. (*R*)-**2** was used to investigate interactions with (*R*,*R*)- and (*S*,*S*)-CHDA with association data obtained by using a range of techniques summarized in Table 1. Association constants and selectivity of CHDA binding show good consistency across UV-vis, CD, fluorescence emission and NMR spectroscopy measurements. For all measurements the 1:1 host-guest binding model [26,27] was adopted for comprehensive analysis of the binding process between **2** and CHDA.

The electronic absorption spectrum of (*R*)-**2** (Fig. 3(a)) contains an absorption maximum at 410 nm with a shoulder at approximately 425 nm. This is associated with a relatively weak CD signature centered at 425 nm (Fig. 3 (b)). The band at 425 nm present prior to addition of guest is most likely a manifestation of intramolecular stacking of the Zn(TAP) units and also gives rise to the weak CD response because of the orientation of chromophores forced by the 1,1'-binaphthyl unit, as demonstrated in other diporphyrin tweezer systems [40]. After binding of guest, the band at 425 nm is enhanced due to coordination of Zn(II) to CHDA. Binding of (*R*,*R*)-CHDA promotes this orientation of the chromophores giving rise to an enhancement of the UV-vis signal centered at 425 nm and leading to a large enhancement of the CD signal. In contrast, addition of (*S*,*S*)-CHDA switches the orientation of the chromophores (Fig. 3(b)) according to the guest conformation, giving rise to an inversion in the sign of the CD signal. Due to symmetry (*S*)-**2** behaves opposite in a corresponding fashion. Orientation of the chromophores in bis-porphyrin tweezers is known to strongly affect the observed CD signal amplitude and polarity with this feature having been well investigated in other chiral [41] and achiral [18,42] porphyrin dimer tweezers. Our observations are similar to those observed on binding of CHDA to other bis-porphyrinatozinc(II) tweezers. The 1:1 host-guest binding model of (*R*)-**2** with CHDA was confirmed by Job's plot with maximum at $x_H = 0.5$ (Fig. 3(c)). We have also performed SVD analysis of the titration of (*R*)-**2** with (*R*,*R*)- and (*S*,*S*)-CHDA (Figs. S10 and S11 (cf. ESM)). As expected, there are two species present during the whole titration (Fig. 3(d)), which can be assigned to free (*R*)-**2** host (H) and 1:1 (*R*,*R*)-CHDA⊂(*R*)-**2** complex (HG). The binding constants as obtained from UV-vis and CD measurements (in toluene and chloroform) are listed in Table 1.

The fluorescence spectrum of (*R*)-**2** in toluene contains two maxima at 613 nm and 658 nm which, upon CHDA guest binding, increase in intensity and are shifted to 621 nm and 675 nm, respectively (Fig. 4). When the normalized fluorescence intensities at varying equivalents of (*R*,*R*)-CHDA and (*S*,*S*)-CHDA are analyzed, binding constants of the order of 10^5 L·mol^{-1} can be obtained with a selectivity of 2.8 in favour of (*R*,*R*)-CHDA (Table 1). The increase in the fluorescence signal can be attributed to an increase in the intramolecular distance between the two porphyrins, leading to a decrease in quenching and an increase in the fluorescence signal proportional to the binding strengths. Unfortunately, the diastereomeric complex appears to be prone to decomposition when irradiated for prolonged periods of time, this can be seen in the spectra (Fig. 4) by the emergence of a signal at 640 nm. Interestingly the rate of decomposition is dependent upon the guest enantiomer present, where a faster rate of decomposition is observed with (*S*,*S*)-CHDA (complementary observations were found for the other host-guest pair). The decomposition was more pronounced when the solvent was changed to chloroform to such an extent that binding constants could not be determined from the data

Table 1 Association constants for (*R*,*R*)-CHDA and (*S*,*S*)-CHDA as obtained from a range of analytical techniques

Item	Method	K_{RR} /(L·mol^{-1}) for (*R*,*R*)-CHDA	K_{SS} /(L·mol^{-1}) for (*S*,*S*)-CHDA	Selectivity[a] ($K_{RR}\cdot K_{SS}^{-1}$)
(*R*)-**2**, toluene	UV-vis[b]	$7.1\pm0.4\times10^5$	$3.1\pm0.2\times10^5$	2.3
	CD[b]	$7.2\pm0.7\times10^5$	$2.7\pm0.3\times10^5$	2.6
	Fl[b]	$4.2\pm0.8\times10^5$	$1.5\pm0.4\times10^5$	2.8
(*R*)-**2**, chloroform[c]	UV-vis[b]	$7.47\pm0.37\times10^4$	$2.65\pm0.13\times10^4$	2.8
	CD[b]	$9.17\pm1.38\times10^4$	$3.84\pm0.58\times10^4$	2.4
	Fl[b]	n.d.[d]	n.d.[d]	n.d.[d]
	NMR[e]	$8.44\pm2.53\times10^4$	$3.25\pm0.97\times10^4$	2.6

a) Selectivity ($K_{RR}\cdot K_{SS}^{-1}$) is defined as the ratio of larger binding constant of (*R*)-**2** with (*R*,*R*)-CHDA (K_{RR}) divided by smaller binding constant with (*S*,*S*)-CHDA (K_{SS}); b) $[(R)\text{-}\mathbf{2}]_{tot} = 1.0\times10^{-6}$ mol·L^{-1}, all data was recorded at room temperature under ambient conditions; c) For UV-vis and CD spectroscopic titration data see Fig. S3 (cf. ESM); d) Rapid decomposition was observed when samples were irradiated at 410 nm, therefore a binding constant could not be determined; e) $[(R)\text{-}\mathbf{2}]_{tot} = 1.9\times10^{-3}$ mol·L^{-1}, 25°C, for actual binding isotherms see Fig. 5.

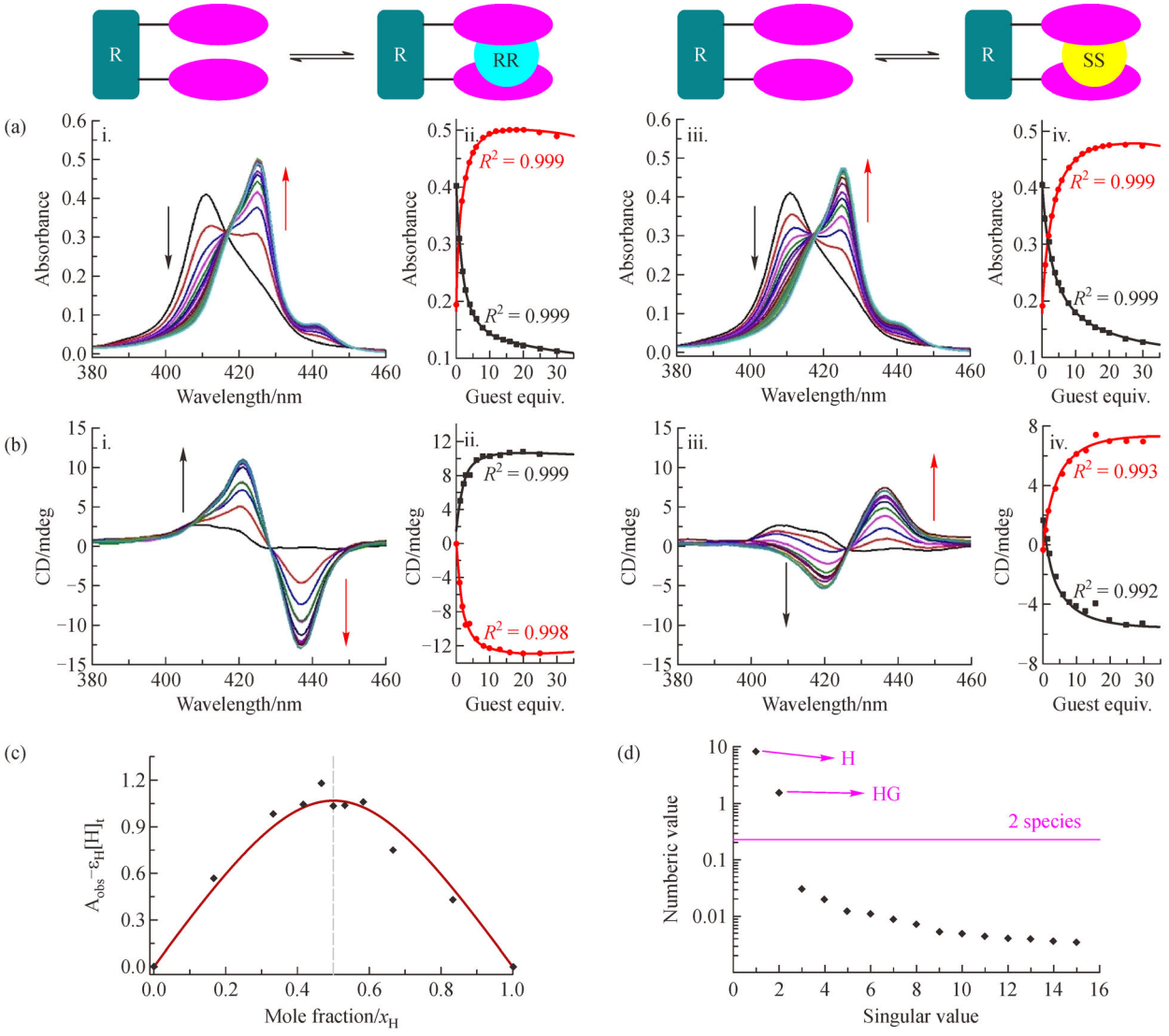

Fig. 3 Titrations of (*R*)-**2** monitored using UV-vis and CD spectroscopy. (a) Titrations monitored using UV-vis spectroscopy: i. (*R*)-**2** (1.0×10^{-6} mol·L^{-1}) with up to 30 equiv. of (*R*,*R*)-CHDA (3.5×10^{-4} mol·L^{-1}) in toluene at room temperature; ii. 1:1 host-guest binding isotherms for the titration of (*R*)-**2** with (*R*,*R*)-CHDA constructed from absorbances at 410 nm (black) and 425 nm (red) and fitted simultaneously; iii. (*R*)-**2** (1.0×10^{-6} mol·L^{-1}) with up to 30 equiv. of (*S*,*S*)-CHDA (3.5×10^{-4} mol·L^{-1}) in toluene at room temperature; iv. 1:1 host-guest binding isotherms for the titration of (*R*)-**2** with (*S*,*S*)-CHDA constructed from absorbances at 410 nm (black) and 425 nm (red) and fitted simultaneously. (b) Titrations monitored by CD spectroscopy: i. (*R*)-**2** (1.0×10^{-6} mol·L^{-1}) with up to 25 equiv. of (*R*,*R*)-CHDA (3.5×10^{-4} mol·L^{-1}) in toluene at room temperature; ii. 1:1 host-guest binding isotherms for the titration of (*R*)-**2** with (*R*,*R*)-CHDA constructed from CD signals at 421 nm (black) and 437 nm (red) and fitted simultaneously; iii. (*R*)-**2** (1.0×10^{-6} mol·L^{-1}) with up to 30 equiv. of (*S*,*S*)-CHDA (3.5×10^{-4} mol·L^{-1}) in toluene at room temperature; iv. 1:1 host-guest binding isotherms for the titration of (*R*)-**2** with (*S*,*S*)-CHDA constructed from CD signals at 410 nm (black) and 425 nm (red) and fitted simultaneously. For the binding constants see Table 1. (c) Job's plot constructed for the binding of (*R*,*R*)-CHDA with (*R*)-**2** (the total concentration was kept constant at $[H]_{tot} + [G]_{tot} = 10^{-5}$ mol·L^{-1}) in toluene monitored at 425 nm at room temperature. *x*-axis shows molar fraction of host $x_H = [H]_{tot} / ([H]_{tot} + [G]_{tot})$. ε_H and $[H]_t$ are molar attenuation coefficient and total concentration of (*R*)-**2**, respectively. The red curve is 1:1 calculated Job's plot using $K_{RR} = 7.1 \times 10^5$ L·mol^{-1} (Table 1) (d) Singular values as obtained from SVD analysis of titration (*R*,*R*)-CHDA into (*R*)-**2** solution.

obtained (see Fig. S4, cf. ESM)). Decomposition appears to be due to demetallation of the Zn(TAP) moieties since the fluorescence emission band emerging at 640 nm is at a relative wavelength characteristic of non-metallated porphyrin free bases [43]. The greater stability of the complex with (*R*,*R*)-CHDA suggests that decomposition is more rapid in the non-complexed host molecule.

^{1}H NMR Spectroscopy. NMR titrations were performed in order to probe the binding properties at higher (*R*)-**2** host concentration (ca. 10^{-3} mol·L^{-1}), see Fig. 5(a) and Fig. S5

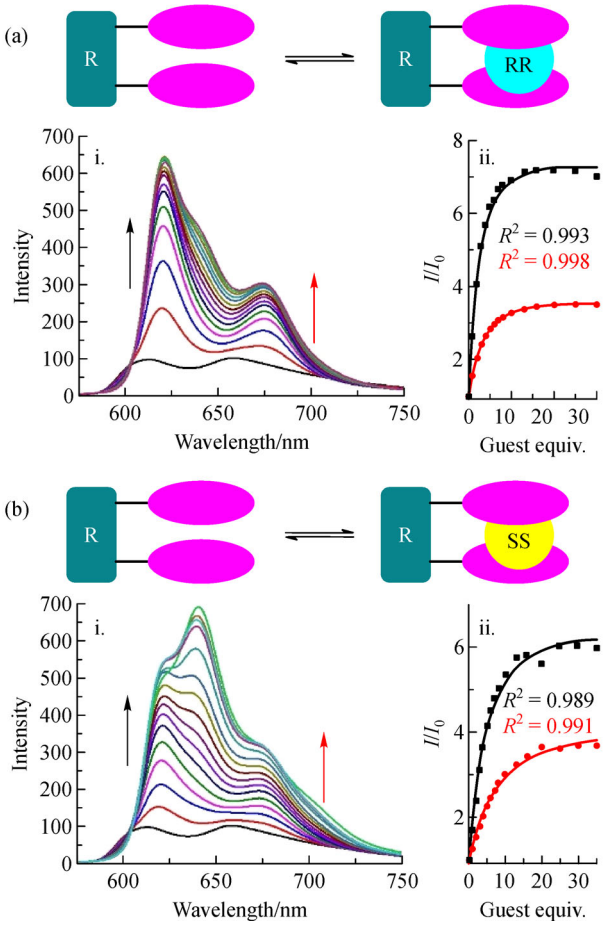

Fig. 4 Titrations of (*R*)-**2** monitored using fluorescence spectroscopy. (a) Titration of (*R*)-**2** (1.0×10^{-6} mol·L^{-1}) with (*R*,*R*)-CHDA (3.5×10^{-4} mol·L^{-1}) in toluene at room temperature monitored by fluorescence spectroscopy at $\lambda_{ex} = 410$ nm: i. Addition of 0–30 equiv. of (*R*,*R*)-CHDA; ii. Binding isotherms for the titration of (*R*)-**2** with (*R*,*R*)-CHDA constructed from normalized fluorescence at 621 nm (black) and 675 nm (red) and fitted simultaneously (solid lines) using 1:1 host-guest model; (b) Titration of (*R*)-**2** (1.0×10^{-6} mol·L^{-1}) with (*S*,*S*)-CHDA (3.5×10^{-4} mol·L^{-1}) in toluene at room temperature monitored by fluorescence spectroscopy at $\lambda_{ex} = 410$ nm: i. Addition of 0–35 equiv. of (*S*,*S*)-CHDA; ii. Binding isotherms for the titration of (*R*)-**2** with (*S*,*S*)-CHDA constructed from normalized fluorescence at 621 nm (black) and 675 nm (red) and fitted simultaneously (solid lines) using 1:1 host-guest model. For binding constants see Table 1.

(cf. ESM). The experimental binding isotherms were constructed from two selected resonances (one corresponding to host, see Figs. S6 and S7 (cf. ESM) for ^{1}H NMR assignments, and one to guest) as shown in Figs. 5(b) and 5(c) and indicate that the stoichiometry is 1:1, which was confirmed with Job's plot (Fig. 5(d)). Therefore, a 1:1 model was adopted for fitting of the NMR data [26,27]. Obtained binding constants are listed in Table 1.

Having successfully determined that (*R*)-**2** can be used to distinguish between the enantiomers of CHDA using UV-vis, CD, fluorescence or NMR spectroscopy, we generated the corresponding *ee* calibration curves in order that *ee* values of unknown samples might be determined using these methods. This was achieved through the addition of 2 or 20 equiv. aliquots of CHDA of varying *ee* to a solution of (*R*)-**2** (1×10^{-6} mol·L^{-1}) in toluene. The responses of the solutions were then measured with the aforementioned techniques and were plotted as calibration curves, which are shown in Fig. 6. All three optical techniques give good resolution of *ee* with reasonable sensitivity considering the low concentrations used (ca. 10^{-6} mol·L^{-1}). There are several limitations present in the system, such as independent calibration curves are required depending on the number of equivalent of analyte added, due to inherent chirality in the host a CD signal is present in the absence of a guest and the differences in binding strength between enantiomers leads to a CD response in the presence of a racemic guest. The *ee* determination of CHDA enantiomers using NMR spectroscopy is also possible because of the reasonably well separated resonances of (*R*,*R*)- and (*S*,*S*)-CHDA (Fig. S5, cf. ESM)). However, although NMR can be a very useful

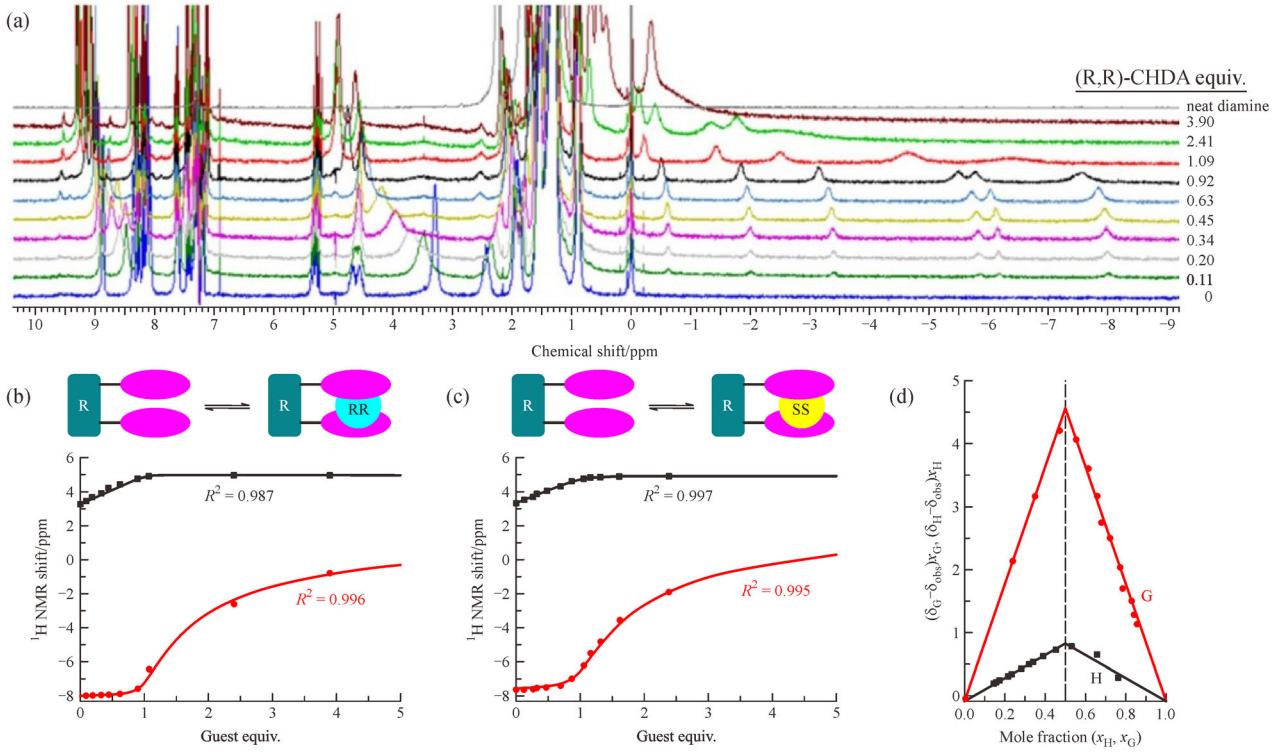

Fig. 5 Interrogation of (*R*)-**2** binding by NMR spectroscopy. (a) Titration of (*R*)-**2** (1.9×10^{-3} mol·L^{-1}) with 0–3.9 equiv. of (*R*,*R*)-CHDA (0.1 mol·L^{-1}) in chloroform-*d* monitored by ^{1}H NMR spectroscopy at 25°C; (b) Binding isotherms for the titration of (*R*)-**2** with (*R*,*R*)-CHDA constructed from resonances at 3.3 ppm (black) and –8.02 ppm (red) and fitted simultaneously (solid lines) using 1:1 host-guest model; (c) Binding isotherms for the titration of (*R*)-**2** with (*S*,*S*)-CHDA constructed from resonances at 3.3 ppm (black) and –7.65 ppm (red) and fitted simultaneously (solid lines) using 1:1 host-guest model. For actual binding constants see Table 1. (d) Jobs plot for the titration of (*R*)-**2** with (*R*,*R*)-CHDA in chloroform-*d* constructed from two resonances at δ_H = 3.3 ppm corresponding to host (H) (black) and δ_G = –8.02 ppm corresponding to guest (G) (red). The total concentration was kept constant at $[H]_{tot} + [G]_{tot} = 6\times10^{-3}$ mol·L^{-1}. *x*-axis shows molar fraction of host $x_H = [H]_{tot} / ([H]_{tot} + [G]_{tot})$ and guest $x_G = [G]_{tot} / ([H]_{tot} + [G]_{tot})$ depending on the corresponding resonance used.

method for *ee* determination [44], in this case only the resonances around-6 ppm can be used for this purpose with moderate accuracy.

The application of porphyrins dimers for chiral analysis has been well established through the work of Borovkov, Inoue and coworkers as well as by Berova, and bis-porphyrins remain an important structural motif for the study of the consequences of supramolecular chirality [18,34,35,40–42,45–47]. In this case, we also have the benefit of being able to compare our results with another recently reported porphyrin dimer host system [47]. The *meso*-tetraphenylporphyrin (TPP) analogue of our system can also be used for chiral discrimination. The properties of that system have been investigated by Lu et al. [47]. They found that enantiomers of CHDA can be easily discriminated using their host molecules. This is mirrored in our work using NMR spectroscopy. We provide the additional analytical possibility of calibration for *ee* determination using UV-vis (as well as CD and fluorescence emission). For UV-vis purposes, the use of TAP over TPP has the advantage of shifting the UV_{max} of our host to shorter wavelength relative to the diamine complex facilitating construction of *ee* calibration plots. We also illustrate the use of fluorescence emission for *ee* determination although this is complicated by the photo-induced demetallation of the host (markedly promoted when chloroform is used as solvent). Despite this, we expect that other highly fluorescent tetrapyrrole derivatives will be found to be more suitable for the construction of fluorescent *ee* sensors in the near future.

4 Conclusions

In summary, we have investigated chiral discrimination and *ee* determination in binaphthyl-linked diporphyrin tweezers using as model chiral guests the enantiomers of 1,2-CHDA. These studies have resulted in the construction of *ee* calibration curves for different spectroscopic techniques including UV-vis, CD and fluorescence emission spectrophotometries. The availability of strongly fluorescent aromatic macrocycles derived from tetrapyr-

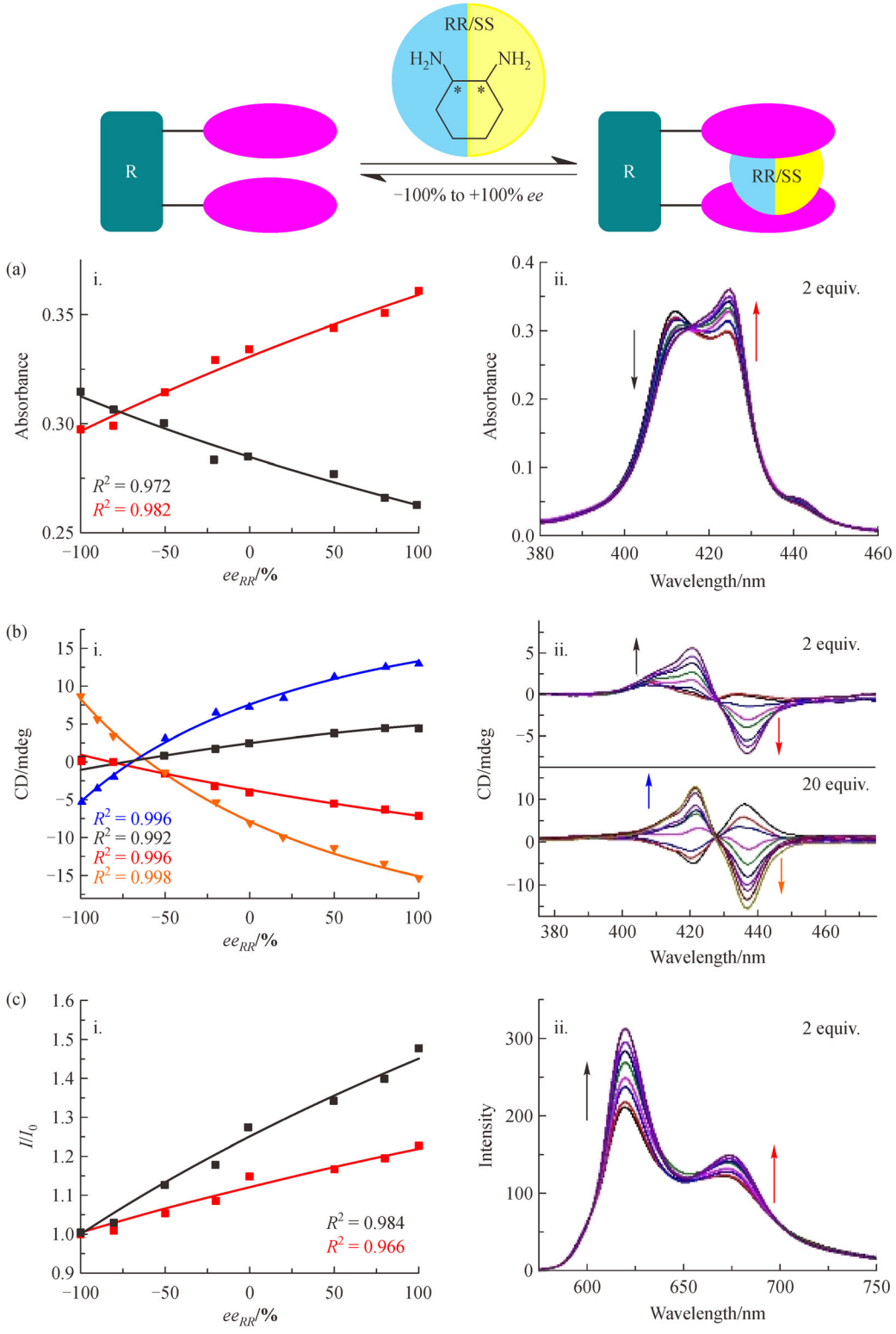

Fig. 6 Calibration curves to determine ee_{RR} using (*R*)-**2** host molecule (subscript '*RR*' indicates that the *ee* values are taken with respect to (*R*,*R*)-CHDA). (a) Calibration using UV-vis spectroscopy: i. Calibration isotherms for various ee_{RR} solutions of CHDA (2 equiv.) with (*R*)-**2** (1.0×10^{-6} mol·L^{-1}) host constructed from absorbances at 410 nm (black) and 425 nm (red); ii. UV-vis spectra during the addition of 2 equiv. of various ee_{RR} of CHDA to (*R*)-**2** (1.0×10^{-6} mol·L^{-1}) host solution at room temperature. (b) Calibration using CD spectroscopy: i. Calibration isotherms for various ee_{RR} of CHDA with (*R*)-**2** (1.0×10^{-6} mol·L^{-1}) host constructed from CD signals at 421 nm (black and blue, respectively, for 2 and 20 equiv. of CHDA) and 437 nm (red and orange, respectively, for 2 and 20 equiv. of CHDA); ii. CD spectra during the addition of 2 equiv. (top) and 20 equiv. (bottom) of various ee_{RR} of CHDA to (*R*)-**2** (1.0×10^{-6} mol·L^{-1}) host solution at room temperature. (c) Calibration using fluorescence spectroscopy: i. Calibration isotherms for various ee_{RR} solutions of CHDA (2 equiv.) with (*R*)-**2** (1.0×10^{-6} mol·L^{-1}) host constructed from normalized fluorescence signals at 621 nm (black) and 675 nm (red); ii. Fluorescence spectra during the addition of various ee_{RR} of CHDA (2 equiv.) to (*R*)-**2** (1.0×10^{-6} mol·L^{-1}) host solution at room temperature. Note: The arrows direction indicate the change of ee_{RR} from −100% to + 100%.

roles makes it highly likely that modifications of the system reported here will lead to compounds with improved chiral selectivity and *ee* reporting ability especially using the fluorescence channel in combination with unsymmetrically substituted 1,1'-binaphthyl derivatives. We will report on our analyses of these systems in the near future.

Acknowledgements This work was partly supported by World Premier International Research Center Initiative, MEXT, Japan. The authors are grateful to Japan Society for the Promotion of Science (JSPS) for a JSPS Fellowship (to D.T.P.). This work was also partially supported by JSPS KAKENHI (Coordination Asymmetry) Grant No. JP16H06518, JSPS KAKENHI Grant No. 19K05229 and CREST, JST Grant No. JPMJCR1665. This work was partly financially supported by the National Science Foundation (Grant No. 1401188 to FD). The authors thank the Catalysis and Sensing for our Environment network for essential networking opportunities [48].

Electronic Supplementary Material Supplementary material is available in the online version of this article at https://doi.org/10.1007/s11705-019-1869-1 and is accessible for authorized users.

References

1. Nunez M D C, Gallo M A, Espinosa A, Campos J M. Rapid development of chiral drugs in the pharmaceutical industry. In: New Developments in Medicinal Chemistry. United Arab Emirates: Bentham Science Publishers, 2010, 95–113
2. Lehn J M. Supramolecular Chemistry: Concepts and Perspectives. Weinheim, Germany: Wiley-VCH Verlagsgesellschaft, 1995, 1–271
3. Halpern J, Trost B. Asymmetric catalysis. Proceedings of the National Academy of Sciences of the United States of America, 2004, 101(15): 5347
4. Okamoto Y, Ikai T. Chiral HPLC for efficient resolution of enantiomers. Chemical Society Reviews, 2008, 37(12): 2593–2608
5. Parker D. NMR determination of enantiomeric purity. Chemical Reviews, 1991, 91(7): 1441–1457
6. Shcherbakova E G, Brega V, Lynch V M, James T D, Anzenbacher P Jr. High-throughput assay for enantiomeric excess determination in 1,2- and 1,3-diols and direct asymmetric reaction screening. Chemistry (Weinheim an der Bergstrasse, Germany), 2017, 23(42): 10222–10229
7. Jo H H, Lin C Y, Anslyn E V. Rapid optical methods for enantiomeric excess analysis: From enantioselective indicator displacement assays to exciton-coupled circular dichroism. Accounts of Chemical Research, 2014, 47(7): 2212–2221
8. Yang L, Wenzel T, Williamson R T, Christensen M, Schafer W, Welch C J. Expedited selection of NMR chiral solvating agents for determination of enantiopurity. ACS Central Science, 2016, 2(5): 332–340
9. Pirkle W H, Sikkenka D L. The use of chiral solvating agent for nuclear magnetic resonance determination of enantiomeric purity and absolute configuration of lactones: Consequences of three-point interactions. Journal of Organic Chemistry, 1977, 42(8): 1370–1374
10. Labuta J, Ishihara S, Šikorský T, Futera Z, Shundo A, Hanyková L, Burda J V, Ariga K, Hill J P. NMR spectroscopic detection of chirality and enantiopurity in referenced systems without formation of diastereomers. Nature Communications, 2013, 4(1): 2188
11. Labuta J, Hill J P, Ishihara S, Hanyková L, Ariga K. Chiral sensing by nonchiral tetrapyrroles. Accounts of Chemical Research, 2015, 48(3): 521–529
12. Kadish K M, Smith K M, Guilard R, eds. The Porphyrin Handbook. San Diego: Academic Press, 2003, 1–20
13. Sreenilayam G, Moore E J, Steck V, Fasan R. Stereoselective olefin cyclopropanation under aerobic conditions with an artificial enzyme incorporating an iron-chlorin e6 cofactor. ACS Catalysis, 2017, 7(11): 7629–7633
14. Nandipati V, Akinapelli K, Koya L, Starnes S D. Recognition of mandelate stereoisomers by chiral porphyrin hosts: Prediction of stereopreference in guest binding a priori using a simple binding model. Tetrahedron Letters, 2014, 55(5): 985–991
15. Ema Y, Nemugaki S, Tsuboi S, Utaka M. Synthesis and CD spectrum of chiral porphyrin dimer. Tetrahedron Letters, 1995, 36(33): 5905–5908
16. Hayashi T, Nonoguchi M, Aya T, Ogoshi H. Molecular recognition of α,ω-diamines by metalloporphyrin dimer. Tetrahedron Letters, 1997, 38(9): 1603–1606
17. Kurtán T, Nesnas N, Li Y Q, Huang X, Nakanishi K, Berova N. Chiral recognition by CD-sensitive dimeric zinc porphyrin host. 1. Chiroptical protocol for absolute configurational assignments of monoalcohols and primary monoamines. Journal of the American Chemical Society, 2001, 123(25): 5962–5973
18. Borovkov V V, Fujii I, Muranaka A, Hembury G A, Tanaka T, Ceulemans A, Kobayashi N, Inoue Y. Rationalization of supramolecular chirality in a bisporphyrin system. Angewandte Chemie International Edition, 2004, 43(41): 5481–5485
19. Saha B, Ikbal S A, Petrovic A G, Berova N, Rath S P. Complexation of chiral zinc-porphyrin tweezer with achiral diamines: Induction and two-step inversion of interporphyrin helicity monitored by ECD. Inorganic Chemistry, 2017, 56(7): 3849–3860
20. Liu G, Yasumitsu T, Zhao L, Peng X, Wang F, Bauri A K, Aonuma S, Kimura T, Komatsu N. Preferential extraction of left- and right-handed single-walled carbon nanotubes by use of chiral diporphyrin nanotweezers. Organic & Biomolecular Chemistry, 2012, 10(30): 5830–5836
21. Labuta J, Ishihara S, Shundo A, Arai S, Takeoka S, Ariga K, Hill J P. Chirality sensing by non-chiral porphines. Chemistry (Weinheim an der Bergstrasse, Germany), 2011, 17(13): 3558–3561
22. Ishihara S, Labuta J, Futera Z, Mori S, Sato H, Ariga K, Hill J P. NMR spectroscopic determination of enantiomeric excess using small prochiral molecules: Intermolecular transfer of magnetic anisotropy in isotropic media. Journal of Physical Chemistry B, 2018, 122(19): 5114–5120
23. Shinoda T, Onaka M, Izumi Y. The reason why K10 is an effective promoter for meso-tetraalkylporphyrin synthesis. Chemistry Letters, 1995, 24(7): 493–494
24. Plamont R, Kikkawa Y, Takahashi M, Kanesato M, Giorgi M, Shun A C K, Roussel C, Balaban T S. Nanoscopic imaging of meso-tetraalkylporphyrins prepared in high yields enabled by Montmorillonite K10 and 3 Å molecular sieves. Chemistry (Weinheim an der Bergstrasse, Germany), 2013, 19(34): 11293–11300
25. Rostami M, Rafiee L, Hassanzadeh F, Dadrass A R, Khodarahmi G

A. Synthesis of some new porphyrins and their metalloderivatives as potential sensitizers in photo-dynamic therapy. Research in Pharmaceutical Sciences, 2015, 10(6): 504–513
26. Connors K A. Binding Constants: The Measurement of Molecular Complex Stability. New York: Wiley-Interscience, 1987, 1–432
27. Hirose K. A practical guide for the determination of binding constants. Journal of Inclusion Phenomena and Macrocyclic Chemistry, 2001, 39(3-4): 193–209
28. Henry E R, Hofrichter J. Methods in Enzymology. London: Academic Press, 1992, 210: 29–192
29. Malinowski E R. Factor Analysis in Chemistry. New York: Wiley-Interscience, 2002, 1–432
30. Březina V, Ishihara S, Lang J, Hanyková L, Ariga K, Hill J P, Labuta J. Structural modulation of chromic response: Effects of binding-site blocking in a conjugated calix[4]pyrrole chromophore. ChemistryOpen, 2018, 7(5): 323–335
31. Hanuš J, Chmelová K, Štěpánek J, Turpin P Y, Bok J, Rosenberg I, Točík Z. Raman spectroscopic study of triplex-like complexes of polyuridylic acid with the isopolar, non–isosteric phosphonate analogues of diadenosine monophosphate. Journal of Raman Spectroscopy, 1999, 30(8): 667–676
32. Zimányi L. Analysis of the bacteriorhodopsin photocycle by singular value decomposition with self-modeling: A critical evaluation using realistic simulated data. Journal of Physical Chemistry B, 2004, 108(13): 4199–4209
33. Zimányi L, Kulcsár Á, Lanyi J K, Sears D F, Saltiel J. Singular value decomposition with self-modeling applied to determine bacteriorhodopsin intermediate spectra: Analysis of simulated data. Proceedings of the National Academy of Sciences of the United States of America, 1999, 96(8): 4408–4413
34. Brahma S, Ikbal S A, Dhamija A, Rath S P. Highly enhanced bisignate circular dichroism of ferrocene-bridged Zn(II) bisporphyrin tweezer with extended chiral substrates due to well-matched host-guest system. Inorganic Chemistry, 2014, 53(5): 2381–2395
35. Brahma S, Ikbal S A, Rath S P. Synthesis, structure, and properties of a series of chiral tweezer-diamine complexes consisting of an achiral zinc(II) bisporphyrin host and chiral diamine guest: Induction and rationalization of supramolecular chirality. Inorganic Chemistry, 2014, 53(1): 49–62
36. Zhang P, Wolf C. Sensing of the concentration and enantiomeric excess of chiral compounds with tropos ligand derived metal complexes. Chemical Communications, 2013, 49(62): 7010–7012
37. Jung S H, Kim K Y, Ahn A, Lee S S, Choi M Y, Jaworski J, Jung J W. NMR detection of chirality and enantiopurity of amines by using benzene tricarboxamide-based hydrogelators as chiral solvating agents. New Journal of Chemistry, 2016, 40(9): 7917–7922
38. Wang C, Wu X, Pu L. A highly fluorescent chiral aldehyde for enantioselective fluorescent recognition in a biphasic system. Chemistry (Weinheim an der Bergstrasse, Germany), 2017, 23(45): 10749–10752
39. Zardi P, Wurst K, Licini G, Zonta C. Concentration-independent stereodynamic *g*-Probe for chiroptical enantiomeric excess determination. Journal of the American Chemical Society, 2017, 139(44): 15616–15619
40. Ema T, Ouchi N, Doi T, Korenaga T, Sakai T. Highly sensitive chiral shift reagent bearing two zinc porphyrins. Organic Letters, 2005, 7(18): 3985–3988
41. Ema T, Misawa S, Nemugaki S, Sakai T, Utaka M. New optically active diporphyrin having a chiral cyclophane as a spacer. Chemistry Letters, 1997, 26(6): 487–488
42. Borovkov V V, Lintuluoto J M, Hembury G A, Sugiura M, Arakawa R, Inoue Y. Supramolecular chirogenesis in zinc porphyrins: Interaction with bidentate ligands, formation of tweezer structures, and the origin of enhanced optical activity. Journal of Organic Chemistry, 2003, 68(19): 7176–7192
43. Chen Q, Hirsch R E. A direct and simultaneous detection of zinc protoporphyrin IX, free protoporphyrin IX, and fluorescent heme degradation product in red blood cell hemosylates. Free Radical Research, 2006, 40(3): 285–294
44. Fossey J S, Anslyn E V, Brittain W D G, Bull S D, Chapin B M, Le Duff C L, James T D, Lees G, Lim S, Lloyd J A C, et al. Rapid determination of enantiomeric excess via NMR spectroscopy: A research-informed experiment. Journal of Chemical Education, 2017, 94(1): 79–84
45. Berova N, Pescitelli G, Petrovic A G, Proni G. Probing molecular chirality by CD-sensitive dimeric metalloporphyrin hosts. Chemical Communications, 2009, 40(40): 5958–5980
46. Tanasova M, Anyika M, Borhan B. Sensing remote chirality: Stereochemical determination of β, γ, and δ-chiral carboxylic acids. Angewandte Chemie International Edition, 2015, 54(14): 4274–4278
47. Lu W, Yang H, Li X, Wang C, Zhan X, Qi D, Bian Y, Jiang J. Chiral discrimination of diamines by a binaphthylene-bridged porphyrin dimer. Inorganic Chemistry, 2017, 56(14): 8223–8231
48. Payne D T, Fossey J S, Elmes R B P. Catalysis and sensing for our environment (CASE2015) and the supramolecular chemistry Ireland meeting (SCI 2015): Dublin and Maynooth, Ireland. 8th–11th July. Supramolecular Chemistry, 2016, 28(11-12): 921–931